

Flow-driven collapse of lubricant-infused surfaces

By Evgeny S. Asmolov^{1,2}, Tatiana V. Nizkaya¹ and Olga I. Vinogradova^{1,2,3} †

¹A.N. Frumkin Institute of Physical Chemistry and Electrochemistry,
Russian Academy of Sciences, 31 Leninsky Prospect, 119071 Moscow, Russia

²M. V. Lomonosov Moscow State University, 119991 Moscow, Russia

³DWI - Leibniz Institute for Interactive Materials, Forckenbeckstr. 50, 52056 Aachen, Germany

(Received Received: date / Accepted: date)

Lubricant-infused surfaces in an outer liquid flow generally reduce viscous drag. However, owing to the meniscus deformation, that it is mostly controlled by the inner lubricant flow, the infused state could collapse. Here we discuss the transition between infused and collapsed states of transverse shallow grooves, considering the capillary number, liquid/lubricant viscosity ratio and aspect ratio of the groove as parameters for inducing this transition. It is found that depending on the depth of the grooves, two different scenarios occur. Generally, a collapse of lubricant-infused surfaces happens due to a depinning of the meniscus from the front groove edge, which is induced by high pressure gradient in the lubricant. However, for very shallow textures, the meniscus contacts the bottom wall before such a depinning could occur. Our interpretation could help avoiding this generally detrimental effect in various applications.

1. Introduction

Slippery lubricant-infused surfaces have received much attention in recent years since they provide a drag reduction and flow manipulation in microfluidic devices (Wong *et al.* 2011; Nizkaya *et al.* 2014; Solomon *et al.* 2014; Keiser *et al.* 2017). The lubricant could be a gas trapped by superhydrophobic (SH) textures or another liquid, such as oil. SH surfaces show very large effective slip length (Ybert *et al.* 2007; Vinogradova & Belyaev 2011), which makes them attractive for use in microfluidic applications (Vinogradova & Dubov 2012). Liquid-infused (LI) surfaces are less slippery (Asmolov *et al.* 2018), but are commonly considered to be potentially more stable and robust against pressure-induced failure compared to SH surfaces, which makes them useful in various applications, including anti-biofouling (Epstein *et al.* 2012) and ice-phobicity (Kim *et al.* 2012). Implementation of LI surfaces often requires a thorough understanding of the dynamics of a lubricant within a patterned substrate that is exposed to external hydrodynamic flow. This fundamental problem also applies to a variety of similar situations, including the stability of small bubbles or droplets, trapped by slightly rough or heterogeneous surfaces (Vinogradova *et al.* 1995; Borkent *et al.* 2007).

The influence of a curved meniscus on the slipping properties of SH texture has been extensively studied analytically (Sbragaglia & Prosperetti 2007), numerically (Teo & Khoo 2010) and in experiments (Karatay *et al.* 2013; Xue *et al.* 2015). In all these studies protrusion or inflection of the meniscus has been achieved by changing the hydrostatic pressure in gas, but the flow-induced dynamic deformations of the meniscus has been neglected. Deformation of liquid/gas interface by the flow has been studied only for strongly protruding bubbles (Gao & Feng 2009; Hyväluoma & Harting 2008). In particular, simulation studies (Hyväluoma & Harting 2008) have

† Author to whom correspondence should be addressed; email: oivinograd@yahoo.com

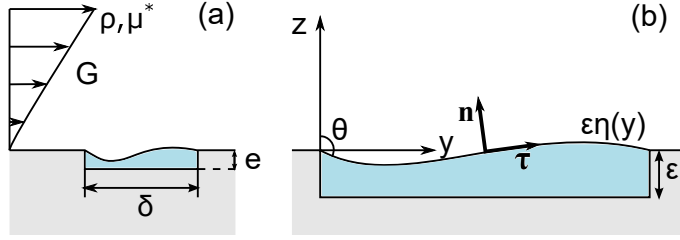


FIGURE 1. Sketches of (a) an outer shear flow past a shallow lubricant-infused groove of with δ and depth e , and of (b) liquid/lubricant interface $\varepsilon\eta(y)$ in dimensionless coordinates. We denote θ as the angle between the vertical and the tangent to the liquid/lubricant interface at the groove front edge.

shown that at large capillary numbers pinned surface bubbles are deformed by an external viscous flow, which dramatically alters the slip length of the SH texture, but no attempt has been made to address the issue of their stability. We are also unaware of any study of the dynamic deformation of an initially flat meniscus.

Existing theories describing a stability of lubricant-infused state mostly include the configurations of static wetting drops at the SH surface. Several static criteria have been suggested (Cottin-Bizonne *et al.* 2004; Bico *et al.* 2002), and later extended to a more complex, metastable situations (Reyssat *et al.* 2008; Dubov *et al.* 2015). The body of theoretical and experimental work investigating the stability of SH and LI surfaces in external flows is rather scarce, although there exists some recent literature in the area. Wexler *et al.* (2015); Liu *et al.* (2016) have considered an outer shear flow aligned with the direction of extended closed grooves, where a reverse pressure gradient in a lubricant is generated. As a result, a curvature of the static meniscus is largest near the channel inlet, and the failure of deep LI grooves occurs when the dynamic contact angle becomes large, while that of shallow grooves - when the meniscus contacts the groove bottom. The collapse of partially filled deep SH and LI grooves induced by an external transverse shear has been studied numerically by Ge *et al.* (2018). These authors concluded that the induced by such a flow meniscus deformation grows with the outer liquid/lubricant viscosity ratio and that the collapse of lubricant-infused grooves is possible only when this ratio exceeds unity.

In this paper we present some results of a study of the possible collapse of shallow lubricant-infused grooves driven by an external transverse shear flow. Our model assumes that the meniscus is initially flat and pinned at the groove edges. We shall see that flow, induced in a lubricant layer, strongly depends on its local thickness, which is in turn controlled by a local pressure gradient, and that the stationary shape of a deformed meniscus becomes concave-convex. The meniscus depinning from the front groove edge occurs when the advancing contact angle for an outer liquid is reached at some critical capillary number. However, very shallow lubricant-infused textures collapse when the deformed meniscus contacts the groove bottom.

The paper is arranged as follows. In Sec. 2 we describe the model of a lubricant-infused shallow groove and derive asymptotic equations for a two-phase flow problem. Sec. 3 contains results of our numerical calculations. We conclude in Sec. 4. The calculation details of the meniscus shape and of the effective slip length are given in Appendix A.

2. Asymptotic theory

We consider a linear flow of an outer liquid of viscosity μ^* over a shallow groove of width δ and depth $e \ll \delta$ (see Fig.1(a)), filled with a lubricant of viscosity μ^{l*} (hereafter the asterisk denotes dimensional variables). The y^* -axis is aligned with the shear direction, while the z^* -axis is defined normal to the wall, and the dimensionless coordinates are introduced as $y = y^*/\delta$ and $z = z^*/\delta$. We assume that the groove aspect ratio is small, $\varepsilon = e/\delta \ll 1$, and that at rest the static

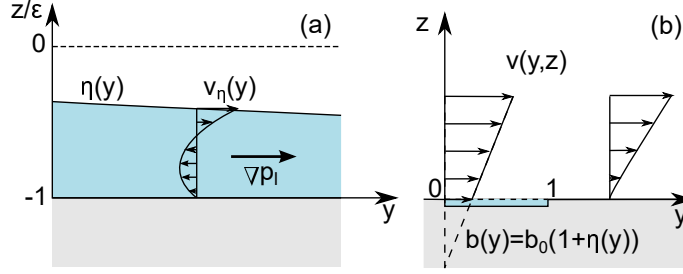


FIGURE 2. (a) Recirculation flow in a shallow groove. (b) Shear flow and a local slip length in outer fluid.

liquid/lubricant interface is flat and located at $z = 0$, i.e. there is no pressure difference across the meniscus. In the presence of external flow the meniscus becomes slightly deformed (see Fig.1(b)), and its shape could be described by a function $\varepsilon\eta(y)$, where $\eta = O(1)$. This implies that the contact angle θ , defined relative to a vertical front wall, decreases compared to that in the static state.

The dimensionless velocity and pressure are defined as $\mathbf{u} = \mathbf{u}^*/(G\delta)$ and $p = p^*/(G\mu^*)$, where G is an undisturbed shear rate. We stress, that near the groove the outer flow is modified due to a slippage at the liquid/lubricant interface, and that the lubricant flow, induced by a reverse pressure gradient, has zero flow rate in any cross-section (see Fig. 2 (a)).

The flows both in lubricant and in outer liquid are governed by Stokes equations,

$$\nabla \cdot \mathbf{u} = 0, \quad \Delta \mathbf{u} - \nabla p = \mathbf{0}, \quad (2.1)$$

$$\nabla \cdot \mathbf{u}^l = 0, \quad \mu \Delta \mathbf{u}^l - \nabla p^l = \mathbf{0}, \quad (2.2)$$

where $\mathbf{u} = (0, v, w)$ and $\mathbf{u}^l = (0, v^l, w^l)$ are velocity fields in liquid and in lubricant, p, p^l are corresponding pressure distributions, and $\mu = \mu^{l*}/\mu^*$ is the lubricant/liquid viscosity ratio. Far from the lubricant-induced surface the liquid flow represents a linear shear flow, $\mathbf{u}|_{z \rightarrow \infty} = z\mathbf{e}_y$, where \mathbf{e}_y is a unit vector along y -axis. We apply no-slip condition at solid boundaries, and at the liquid/lubricant interface, $\varepsilon\eta(y)$, we use the conditions of impermeability

$$\mathbf{u} \cdot \mathbf{n} = \mathbf{u}^l \cdot \mathbf{n} = 0, \quad (2.3)$$

and of continuity of tangent velocity and tangent stresses,

$$\mathbf{u} \cdot \boldsymbol{\tau} = \mathbf{u}^l \cdot \boldsymbol{\tau}, \quad (2.4)$$

$$\boldsymbol{\tau} \cdot \boldsymbol{\sigma} \cdot \mathbf{n} = \boldsymbol{\tau} \cdot \boldsymbol{\sigma}^l \cdot \mathbf{n}, \quad (2.5)$$

where $\boldsymbol{\tau}$ and \mathbf{n} are unit tangent and outward normal (to the meniscus) vectors, and the stress tensors are $\boldsymbol{\sigma} = \nabla \mathbf{u} + (\nabla \mathbf{u})^T - p\mathbf{I}$ and $\boldsymbol{\sigma}^l = \mu \left(\nabla \mathbf{u}^l + (\nabla \mathbf{u}^l)^T \right) - p^l\mathbf{I}$.

The condition for normal stresses at the interface can be derived using the Laplace equation,

$$\mathbf{n} \cdot (\boldsymbol{\sigma}^l - \boldsymbol{\sigma}) \cdot \mathbf{n} = \frac{\kappa}{\text{Ca}}, \quad (2.6)$$

where $\text{Ca} = \mu^*G\delta/\gamma$ is the capillary number defined using an outer liquid viscosity and $\kappa \simeq \varepsilon\eta''$ is the interface curvature (negative for the meniscus protruding into the outer liquid).

These equations should be supplemented by the condition of volume conservation in the lubricant phase and by pinning conditions at the edges of the groove,

$$\int_0^1 \eta(y) dy = 0, \quad \eta(0) = \eta(1) = 0. \quad (2.7)$$

Equations (2.1)-(2.7) represent a closed system governing liquid and lubricant flows. They involve three dimensionless parameters, i.e. the shallow groove aspect ratio ε , and lubricant/liquid viscosity ratio μ , and the capillary number Ca . The two latter parameters could be any, but ε is small, so that we could use it to construct asymptotic solutions for the meniscus shape, velocity fields, and pressure.

Since ε is small, $\boldsymbol{\tau} \simeq (0, 1, \varepsilon \partial_y \eta)$ and $\mathbf{n} \simeq (0, -\varepsilon \partial_y \eta, 1)$, and boundary conditions (2.3)-(2.5) at a curved interface can be simplified to

$$w = w^l = 0, \quad v = v^l = v_\eta(y), \quad \frac{\partial v}{\partial z} = \mu \frac{\partial v^l}{\partial z}, \quad (2.8)$$

which define a coupling between a liquid and a lubricant. Here $v_\eta(y)$ is the tangent velocity of both liquid and lubricant at the interface. From (2.6) we then obtain

$$\sigma_{zz}^l = \sigma_{zz} + \frac{\varepsilon \eta''}{\text{Ca}}, \quad (2.9)$$

which determines the meniscus shape, with normal stresses given by

$$\sigma_{zz} = 2\partial_z w - p, \quad \sigma_{zz}^l = 2\mu \partial_z w^l - p^l. \quad (2.10)$$

Note that the normal stresses include not only the pressure but also gradients of normal velocities since unlike the no-slip case, the latter do not vanish at slippery surfaces.

The lubricant flow in the groove is generated by the interface velocity $v_\eta(y)$. For this inner problem the boundary condition, Eq.(2.8), should be imposed at the curved meniscus $z = \eta(y)$, since its local deviation from the flat one, $z = 0$, is comparable to the depth of the groove, ε . Since the local slopes of the meniscus are small, we apply the lubrication theory and consider a locally parabolic velocity profile of zero flow rate:

$$v^l \simeq v_\eta(y) \zeta (3\zeta - 2), \quad w^l \simeq 0, \quad (2.11)$$

where $\zeta = (z + \varepsilon)/[\varepsilon(1 + \eta)]$ varies from 0 at the bottom wall to 1 at the interface. Eqs.(2.11), which are equivalent to derived by Nizkaya *et al.* (2013) for a flat meniscus, but varying local thickness of the thin lubricant film, allow one to immediately calculate both the lubricant shear rate at the interface

$$\partial_z v^l = \frac{4v_\eta}{\varepsilon(1 + \eta)}. \quad (2.12)$$

and the transverse local slip length

$$b(y) = \frac{v_\eta}{\mu \partial_z v^l} \simeq b_0(1 + \eta), \quad b_0 = \frac{\varepsilon}{4\mu}, \quad (2.13)$$

where $\varepsilon/\mu = O(1)$. Eq.(2.13) implies that $b(y)$ is proportional to a local thickness of the lubricant layer and inversely proportional to μ .

For SH grooves, pressure induced by flow changes in the inner gas is usually neglected since $\mu \ll 1$. However, μ takes on finite values for lubricant-infused surfaces, and the gradient of pressure in closed shallow grooves could become very large, even when the lubricant viscosity is small, $\mu \sim \varepsilon$. Using simple scaling arguments one can show that $\partial_y p^l \simeq \mu \frac{\partial^2 v^l}{\partial y^2} \sim \mu \varepsilon^{-2} \gg 1$. Indeed, the corresponding to Eq.(2.11) pressure profile satisfies

$$\partial_y p^l \simeq \frac{6\mu v_\eta(y)}{\varepsilon^2(1 + \eta)^2}, \quad \partial_z p^l \simeq 0, \quad (2.14)$$

Finally, using (2.14) and (2.2) one can estimate that $2\mu \partial_z w^l \simeq -2\mu \partial_y v^l \sim \mu \ll |p^l|$. From Eqs.(2.10) it then follows that $\sigma_{zz}^l \simeq -p^l$, which may be determined by integrating Eq.(2.14).

We now turn to an outer liquid flow (of length scale δ), that is practically cannot be affected by small variations in $\varepsilon\eta$, and, therefore, Eqs. (2.8) could be mapped to the flat interface, $\mathbf{u}|_{z=\varepsilon\eta} = \mathbf{u}|_{z=0} + O(\varepsilon)$. Impermeability condition Eq.(2.3) is then reduced to $w(y,0) = 0$, and Eq.(2.5) takes the form of a conventional partial slip condition applied at $z = 0$,

$$v = b(y) \frac{\partial v}{\partial z}, \quad (2.15)$$

with the local slip length described by (2.13).

An outer solution for a flow field with prescribed velocity $v_\eta(y)$ and zero normal velocity can be found using $u(y,z)$ for a longitudinal configuration (Asmolov & Vinogradova 2012):

$$v = u + z \frac{\partial u}{\partial z}, \quad w = -z \frac{\partial u}{\partial y}, \quad (2.16)$$

$$p = -2 \frac{\partial u}{\partial y}. \quad (2.17)$$

Here u satisfies the Laplace equation, $\Delta u = 0$, with the boundary condition $u(0,y) = v_\eta(y)$. Eqs. (2.16), (2.17) immediately suggest that $\sigma_{zz}(0,y) = 2\partial_z w - p = 0$. In other words, the contributions of the pressure and the gradient of normal velocity to the normal stress cancel out. This implies that the outer flow does not affect the meniscus deformation.

The equation describing the meniscus shape can be obtained by differentiating Eq. (2.9) with respect to y . Keeping then only the leading term in ε and using Eq. (2.11) we find that this shape obeys

$$\eta''' = -\frac{6\mu\text{Ca}}{\varepsilon^3} \frac{v_\eta(y)}{(1+\eta)^2}. \quad (2.18)$$

To solve this differential equation, conditions (2.7) should be imposed.

To summarize, the outer asymptotic problem is reduced to Eq.(2.1) coupled with the equation for the meniscus shape (2.18) expressed via the local slip length $b(y)$, Eq.(2.13), and interface velocity v_η .

In the general case, the inner and outer flows are strongly coupled, and the two-phase problem should be solved numerically. However, in some limits analytical results could be obtained, thanks to a decoupling of these flows.

In the limit of $\varepsilon/\mu \ll 1$, typical for very viscous lubricant and/or extremely thin lubricant layer, Eq. (2.15) reduces to a no-slip boundary condition, $v(y,0) \simeq 0$. Consequently, an outer flow remains undisturbed by the inner one, and the shear stress in liquid is $\partial_z v(y,0) \simeq 1$. It follows then from (2.8) that the lubricant shear rate is $\partial_z v^l(y,0) \simeq \mu^{-1}$, and the interface velocity, found from Eq. (2.15), is $v_\eta = b(y)\partial_z v(y,0) \simeq \varepsilon(1+\eta)/4\mu$, i.e. it decreases with μ . From Eq.(2.14) it follows then that $\partial_y p^l$ is finite and does not depend on μ , and Eq. (2.18) reduces to

$$\eta''' = -\frac{3\text{Ca}}{2\varepsilon^2(1+\eta)} \quad (2.19)$$

In the opposite limiting case of low lubricant viscosity, $\varepsilon/\mu \gg 1$, the local slip length $b(y)$ is large provided $1+\eta(y)$ remains finite. Thus we might argue that at any deformation a sensible approximation for a local slip would be $b(y) \rightarrow \infty$ that leads to the interface velocity $v_\eta^p(y) = \frac{1}{4} [1 - (2y-1)^2]^{1/2}$ (Philip 1972). Substituting this to Eq.(2.18) we get

$$\eta''' = -\frac{6\mu\text{Ca}}{\varepsilon^3} \frac{v_\eta^p(y)}{(1+\eta)^2}. \quad (2.20)$$

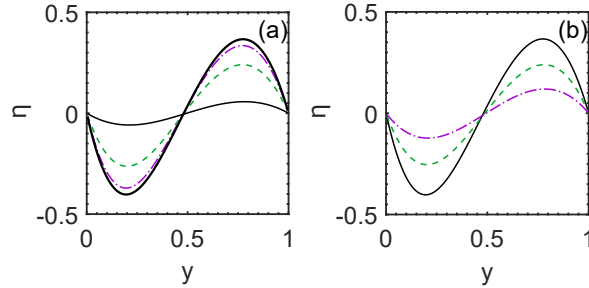


FIGURE 3. (a) Meniscus shape computed at $\varepsilon = 0.1$ and $\text{Ca} = 0.3$. Solid, dashed and dash-dotted curves show results obtained using $\mu = 0.02, 0.2$ and 1 . Bold curve shows calculations from asymptotic Eq.(2.19); (b) Predictions of Eq.(2.19) for $\varepsilon = 0.1$ and $\text{Ca} = 0.1, 0.2, 0.3$ (dash-dotted, dashed and solid curves).

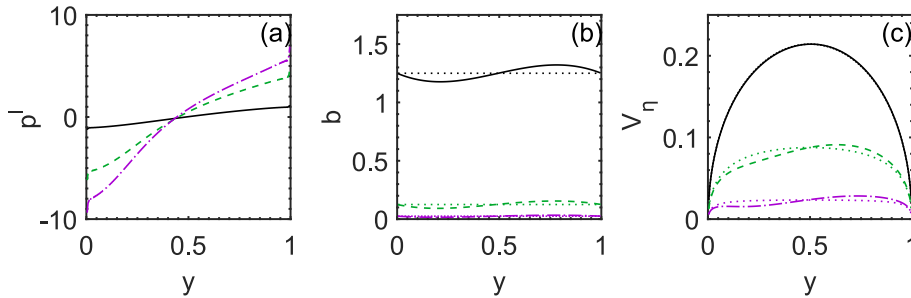


FIGURE 4. (a) Lubricant pressure, (b) local slip length and (c) the interface velocity calculated using $\varepsilon = 0.1$ and $\text{Ca} = 0.3$. Solid, dashed and dash-dotted curves show results for $\mu = 0.02, 0.2$ and 1 . Dotted lines correspond to a flat meniscus.

3. Results of calculations and discussion

In this section we present some numerical results for a model system formulated above. The details of our calculations are presented in Appendix A.

We have first investigated the dynamic meniscus stationary shape, $\eta(y)$, at fixed $\varepsilon = 0.1$. Fig. 3(a) shows the numerical results obtained using $\text{Ca} = 0.3$, and several typical viscosity contrasts, $\mu = 0.02$ (water/air interface), $\mu = 0.2$ (oil/water), and $\mu = 1$, where liquid and lubricant are of the same viscosities. Our calculations show that the function $\eta(y)$ is nearly antisymmetric and has two extrema. It takes its minimum value close to the front edge of the groove (region of concave curvature), and a maximum occurs in the vicinity of the rear edge, where $\eta(y)$ inverts its curvature to convex. The absolute values of extrema decrease with ε/μ , which implies that with our parameters the meniscus deformation grows with μ . Also included are predictions of asymptotic Eq.(2.19), which determines an upper bound on meniscus deformation, attainable for very small ε/μ . For smaller values of Ca , the maximum possible meniscus deformation decreases as illustrated in Fig. 3(b). We also note that a larger deflection of the meniscus shape from the flat one is always accompanied by an increase in $\theta = \pi/2 - \arctan(\eta'(0)/\varepsilon)$.

As described in Sec. 2, the local curvature of the meniscus is associated with pressure in the lubricant film, which in turn can be related to the lubricant flow. Figure 4 plots the lubricant pressure, local slip length $b(y)$ and the interface velocity $v_\eta(y)$ computed with the same parameters as in Fig. 3(a). We see that p^l increases with y , and its gradient is smaller for larger ε/μ , that implies that at fixed ε pressure gradient grows with μ . By contrast, both $b(y)$ and $v_\eta(y)$ increase with ε/μ . The numerical data also show that at large ε/μ the interface velocity remains close to $v_\eta^p(y)$, but for smaller slip lengths it is significantly affected by the deformation of a lubricant film.

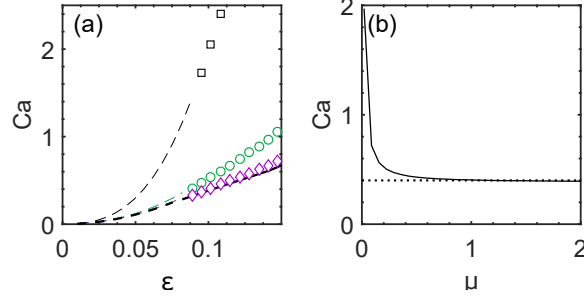


FIGURE 5. (a) Critical values of Ca , beyond which the lubricant-infused surfaces collapse, vs. ε . From top to bottom $\mu = 0.02, 0.2, 1$. Symbols indicate the depinning transitions, dashed curves correspond to a failure caused by a contact of liquid/lubricant interface with a bottom wall. Bold curve shows calculations of depinning (solid curve) and contact (dashed curve) from Eq.(2.19). (b) Critical Ca of depinning as a function of μ calculated using $\varepsilon = 0.1$ (solid curve), and the same calculated from Eq.(2.19) (dotted line).

For a lubricant-infused state to exist, the line of contact must remain pinned. However, the above results suggest that a bigger displacement of liquid/lubricant interface observed when Ca and μ are large enough could eventually allow to reach the threshold, referred to as the advancing, angle θ_a . Beyond the value of θ_a the contact line depins from the groove corner and moves down. To examine this scenario of a collapse more closely, in Fig. 5(a) we denote by symbols in the (Ca, ε) plane the values of Ca , which correspond to $\theta = \theta_a$. Calculations are made at $\varepsilon \geq 0.07$, several fixed μ , taken the same as in Figs. 3 and 4, and using $\theta_a = 2\pi/3$, which is close to observed experimentally for various systems (Dubov *et al.* 2015; Wexler *et al.* 2015). As μ increases the required for a depinning value of Ca reduces, and for sufficiently large μ should approach the value calculated from Eq.(2.19). The curve for the critical Ca of depinning as a function of μ , calculated using $\varepsilon = 0.1$, is included in Fig. 5(b). It can be seen that it reduces rapidly at small viscosity contrast and saturates to a constant value given by Eq.(2.19) already at $\mu \geq 1$. The continuation of the transition line in Fig. 5(a) to smaller ε is not immediate. The reason is that when $\varepsilon \leq 0.07$, the solution of our non-linear system becomes singular for any μ , that indicates another scenario of a collapse of lubricant-infused surfaces. This happens when the local thickness of a lubricant film tends to zero, which is accompanied by an infinite growth of the pressure gradient in the film neck (see Appendix A). Then one might argue that for sufficiently small ε the curve of failure of lubricant-infused surfaces included in Fig. 5(a) reflects a contact of a deformed meniscus with a bottom wall, which occurs before the value of θ_a is reached. It is seen that the curves corresponding to these two scenarios of collapse of lubricant-infused surfaces converge at $\varepsilon \simeq 0.07$.

4. Conclusion

We have studied the meniscus deformation in an outer shear flow oriented transverse to lubricant-infused shallow grooves. It is shown that while such a deformation practically does not affect the slip length, it could induce the collapse of the infused state. We have also shown that unlike the case of deep grooves, for shallow grooves the meniscus deformation increases with μ . The failure of the lubricant-infused surface is controlled by the capillary number Ca , lubricant/liquid viscosity ratio μ , and aspect ratio of the groove ε . Depending on the value of ε two different scenarios occur. Generally, a collapse of lubricant-infused state happens due to a depinning of the meniscus from the front groove edge, induced by high pressure gradient in the lubricant. However, in the case of very small ε , the meniscus contacts the bottom wall before such a depinning could occur.

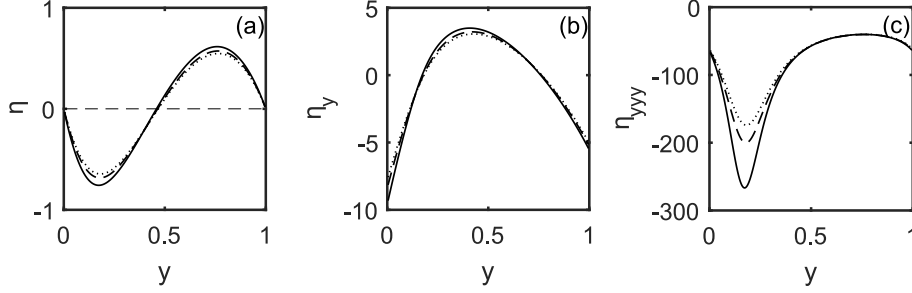


FIGURE 6. (a) Meniscus shape, (b) its first and (c) third derivatives calculated using $\varepsilon/\mu \ll 1$ and $\text{Ca}/\varepsilon^2 = 41.3, 42.3, 43.3$ (dotted, dashed and solid lines).

This research was partly supported by the Russian Foundation for Basic Research (grant 18-01-00729) and the Ministry of Science and Higher Education of the Russian Federation.

Appendix A. Numerical method

The asymptotic equations (2.19) and (2.20) are solved using Runge-Kutta procedure and Newton method to satisfy boundary conditions (2.7). In general case $\varepsilon/\mu = O(1)$, Eqs. (2.1), (2.15) and (2.18) are coupled and we use an iteration scheme, starting from some initial guess. Once the meniscus shape on k -th iteration is known, we solve the Stokes equations in liquid Eq. (2.1) with the local slip length $b^k(y) = b_0[1 + \eta^k(y)]$. We calculate the outer flow for periodical grooves (Nizkaya *et al.* 2013) and expand the solution into Fourier series on a computational domain with a period $L = 5\delta$ (where the solution is no longer dependent on L). The local slip boundary conditions are satisfied using collocation method. The computed interface velocity $v_\eta^k(y)$ is then substituted into the right-hand side of Eq. (2.18) to obtain the next iteration:

$$\frac{\partial^3 \eta^{k+1}}{\partial y^3} = \frac{\mu \text{Ca}}{\varepsilon^3} \frac{6v_\eta^k(y)}{(1 + \eta^k)^2}. \quad (\text{A } 1)$$

The meniscus shape is also sought in terms of Fourier series,

$$\eta(y) = A + B(1 - y)y + \sum_{n=1}^{N_f} [a_n \cos(k_n y) + b_n \sin(k_n y)], \quad (\text{A } 2)$$

where $k_n = 2\pi n$ and A, B, a_n, b_n are a set of $2N_f + 2$ unknown coefficients. To obtain the coefficients a_n, b_n we substitute (A 2) into (2.18) and solve the resulting system of linear equations using the collocation method. Constants A and B are then found from the conditions (2.7): $A = -\sum a_n$, $B = -6(A + 1)$.

If ε is very small, the solution becomes singular when Ca approaches some critical value, which is also quite small. Namely, the smallest local thickness of a lubricant film tends to zero, and simultaneously the pressure gradient diverges. This is illustrated in Fig. 6. We see that the smallest thickness of the lubricant film slightly decreases with the small increase in Ca/ε^2 , but the third derivative of $\eta(y)$, which reflects the growth of pressure gradient in the lubricant neck, changes significantly. Beyond some critical Ca , the solution of positive film thickness does not exist, and our numerical scheme fails to converge.

REFERENCES

- ASMOLOV, E. S., NIZKAYA, T. V. & VINOGRADOVA, O. I. 2018 Enhanced slip properties of lubricant-infused grooves. *Phys. Rev. E* **98**, 033103.

- ASMOLOV, E. S. & VINOGRADOVA, O. I. 2012 Effective slip boundary conditions for arbitrary one-dimensional surfaces. *J. Fluid Mech.* **706**, 108.
- BICO, J., THIELE, U. & QUERE, D. 2002 Wetting of textured surfaces. *Colloids Surfaces A* **206**, 41–46.
- BORKENT, B., DAMMLER, S., SCHONHERR, H., VANSO, G. & LOHSE, D. 2007 Superstability of surface nanobubbles. *Phys. Rev. Lett.* **98**, 204502.
- COTTIN-BIZONNE, C., BARENTIN, C., CHARLAIX, E., BOCQUET, L. & BARRAT, J. L. 2004 Dynamics of simple liquids at heterogeneous surfaces: Molecular-dynamics simulations and hydrodynamic description. *Eur. Phys. J. E* **15**, 489–499.
- DUBOV, A. L., MOURRAN, A., MÖLLER, M. & VINOGRADOVA, O. I. 2015 Regimes of wetting transitions on superhydrophobic textures conditioned by energy of receding contact lines. *Appl. Phys. Lett.* **106**, 241601.
- EPSTEIN, A. K., WONG, T. S., BELISLE, R. A., BOGGS, E. M. & AIZENBERG, J. 2012 Liquid-infused structured surfaces with exceptional anti-biofouling performance. *Proc. Nat. Acad. Sci. U.S.A.* **109**, 13182–13187.
- GAO, P. & FENG, J. J. 2009 Enhanced slip on a patterned substrate due to depinning of contact line. *Phys. Fluids* **21**, 102102.
- GE, Z., HOLMGREN, H., KRONBICHLER, M., BRANDT, L. & KREISS, G. 2018 Effective slip over partially filled microcavities and its possible failure. *Phys. Rev. Fluids* **3** (5), 054201.
- HYVÄLUOMA, J. & HARTING, J. 2008 Slip flow over structured surfaces with entrapped microbubbles. *Phys. Rev. Lett.* **100**, 246001.
- KARATAY, E., HAASE, A. S., VISSER, C. W., SUN, C., LOHSE, D., TSAI, P. A. & LAMMERTINK, R. G. H. 2013 Control of slippage with tunable bubble mattresses. *Proc. Nat. Acad. Sci. U.S.A.* **110**, 8422–8426.
- KEISER, A., KEISER, L., CLANET, C. & QUERE, D. 2017 Drop friction on liquid-infused materials. *Soft Matter* **13**, 6981–6987.
- KIM, P., WONG, T. S., ALVARENGA, J., KREDER, M. J., ADORNO-MARTINEZ, W. E. & AIZENBERG, J. 2012 Liquid-infused nanostructured surfaces with extreme anti-ice and anti-frost performance. *ACS Nano* **6**, 6569–6577.
- LIU, Y., WEXLER, J. S., SCHÖNECKER, C. & STONE, H. A. 2016 Effect of viscosity ratio on the shear-driven failure of liquid-infused surfaces. *Phys. Rev. Fluids* **1**, 074003.
- NIZKAYA, T. V., ASMOLOV, E. S. & VINOGRADOVA, O. I. 2013 Flow in channels with superhydrophobic trapezoidal textures. *Soft Matter* **9**, 11671–11679.
- NIZKAYA, T. V., ASMOLOV, E. S. & VINOGRADOVA, O. I. 2014 Gas cushion model and hydrodynamic boundary conditions for superhydrophobic textures. *Phys. Rev. E* **90** (4), 043017.
- PHILIP, J. R. 1972 Flows satisfying mixed no-slip and no-shear conditions. *J. Appl. Math. Phys.* **23**, 353–372.
- REYSSAT, M., YEOMANS, J. M. & QUERE, D. 2008 Impalement transition of. *Europhys. Lett.* **81**, 26006.
- SBRAGAGLIA, M. & PROSPERETTI, A. 2007 A note on the effective slip properties for microchannel flows with ultrahydrophobic surfaces. *Phys. Fluids* **19**, 043603.
- SOLOMON, B. R., KHALIL, K. S. & VARANASI, K. K. 2014 Drag reduction using lubricant-impregnated surfaces in viscous laminar flow. *Langmuir* **30**, 10970–10976.
- TEO, S. J. & KHOO, B. C. 2010 Flow past superhydrophobic surfaces containing longitudinal grooves: effects of interface curvature. *Microfluid. Nanofluid.* **9**, 499–511.
- VINOGRADOVA, O. I. & BELYAEV, A. V. 2011 Wetting, roughness and flow boundary conditions. *J. Phys.: Condens. Matter* **23**, 184104.
- VINOGRADOVA, O. I., BUNKIN, N. F., CHURAEV, N. V., KISELEVA, O. A., LOBEYEV, A. V. & NINHAM, B. W. 1995 Submicrocavity structure of water between hydrophobic and hydrophilic walls as revealed by optical cavitation. *J. Colloid Interface Sci.* **173**, 443–447.
- VINOGRADOVA, O. I. & DUBOV, A. L. 2012 Superhydrophobic textures for microfluidics. *Mendeleev Commun.* **19**, 229–237.
- WEXLER, J. S., JACOBI, J. & STONE, H. A. 2015 Shear-driven failure of liquid-infused surfaces. *Phys. Rev. Lett.* **114**, 168301.
- WONG, T. S., KANG, S. H., TANG, S. K. Y., SMYTHE, E. J., HATTON, B. D., GRINTHAL, A. & AIZENBERG, J. 2011 Bioinspired self-repairing slippery surfaces with pressure-stable omniphobicity. *Nature* **477**, 443–447.
- XUE, Y., LV, P., LIU, Y., SHI, Y., LIN, H. & DUAN, H. 2015 Morphology of gas cavities on patterned hydrophobic surfaces under reduced pressure. *Phys. Fluids* **27** (9), 092003.

YBERT, C., BARENTIN, C., COTTIN-BIZONNE, C., JOSEPH, P. & BOCQUET, L. 2007 Achieving large slip with superhydrophobic surfaces: Scaling laws for generic geometries. *Phys. Fluids* **19**, 123601.